Magneto-optical and luminescent properties of Tb doped Ge-B-X (X=Ga/La) glasses

Xudong Zhao, Jiadong Li, Weiwei Li, Ping Lu, Mengling Xia, Xianghua Zhang, Xiujian Zhao, Yinsheng Xu

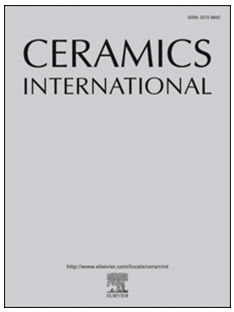

Magneto-optical and luminescent properties of Tb doped Ge-B-X (X=Ga/La) glasses

Xudong Zhao, Jiadong Li, Weiwei Li, Ping Lu, Mengling Xia, Xianghua Zhang, Xiujian Zhao, Yinsheng Xu

PII: S0272-8842(24)00650-3

DOI: https://doi.org/10.1016/j.ceramint.2024.02.154

Reference: CERI 39922

To appear in: *Ceramics International*

Received Date: 27 December 2023

Revised Date: 9 February 2024

Accepted Date: 12 February 2024

Please cite this article as: X. Zhao, J. Li, W. Li, P. Lu, M. Xia, X. Zhang, X. Zhao, Y. Xu, Magneto-optical and luminescent properties of Tb doped Ge-B-X (X=Ga/La) glasses, *Ceramics International* (2024), doi: https://doi.org/10.1016/j.ceramint.2024.02.154.

Magneto-Optical and Luminescent Properties of Tb Doped Ge-B-X (X=Ga/La) Glasses

Xudong Zhao[1,#], Jiadong Li[1,#], Weiwei Li[2], Ping Lu[1,*], Mengling Xia[1], Xianghua Zhang[1,3], Xiujian Zhao[1], Yinsheng Xu[1,*]

[1.] *State Key Laboratory of Silicate Materials for Architectures, Wuhan University of Technology, Wuhan 430070, China*

[2.] *State Key Laboratory of Advanced Technology for Materials Synthesis and Processing, Wuhan University of Technology, Wuhan 430074, China*

[3.] *Institut Des Sciences Chimiques de Rennes UMR 6226, CNRS, Université de Rennes 1, Rennes 35042, France*

E-mail: lupingwh@whut.edu.cn (P. Lu) xuyinsheng@whut.edu.cn (YS Xu)

Abstract

Extensive efforts have been devoted to magneto-optical (MO) glass, owing to its remarkable potential in modern optics, encompassing diverse applications such as optical isolation, modulation, and sensing. Although the Tb ions doped glass has good MO properties, high concentrations of Tb ions tend to cluster, resulting in glass crystallization. To further improve the performance of magneto-optical glass, we must improve the solubility of Tb ions and inhibit the oxidation of paramagnetic Tb^{3+} to diamagnetic Tb^{4+} by adjusting the glass composition. In this work, we conducted a comparative study on GeO_2-B_2O_3-X_2O_3 glasses doped with a fixed concentration of Tb (TGBX, where X represents Ga or La) to elucidate the effects of Ga_2O_3 and La_2O_3 on glass properties. Ga_2O_3 is commonly regarded as a network intermediate, while

La_2O_3 functions as a modifier in glass structure, leading to distinct differences in glass properties and cation valence. Our findings reveal that TGBG glasses exhibit superior MO performance compared to TGBL glasses. Notably, the Verdet constant of TGBG glass with 45 mol.% Tb_2O_3 at 650 nm reaches 105 rad/(T·m). On the other hand, though TGBL glass exhibits a lower Verdet constant, its higher glass network connectivity and a higher concentration of Tb^{3+} ions among Tb ions suggest its potential for preparing larger-sized glasses with an increased Tb molar ratio.

Keywords: Terbium, magneto-optical glass, luminescent property, verdet constant

1. Introduction

Rare earth (RE) elements possess a distinctive role in material design owing to the electronic arrangement in their "f layer". Among these elements, Tb has garnered widespread attention for its luminescent and magneto-optical (MO) properties [1-4]. MO materials play a vital role in various applications in modern optics, including magnetic field sensors, optical isolators, and optical modulators. These materials possess the unique ability to interact with light through the MO effect. Notably, MO crystals and glasses exhibit significantly higher Verdet constants, enabling them to effectively rotate the polarization plane of light by an angle [5-8]. In comparison to crystals, MO glasses offer several advantages. One is their ability to accommodate higher concentrations of Tb ions, thereby improving their MO performance. Additionally, glass can be prepared into a large size and can also be drawn into optical fibers, further expanding its practical applications [9-11]. However, the clustering effect of Tb poses a significant challenge in achieving higher Tb concentrations, as it

leads to glass crystallization. Consequently, it is crucial to determine the doping ability of various glass compositions to increase the doping concentration of Tb ions. Despite this urgent need, few comparative investigations have been undertaken to date to obtain superior glass compositions.

The glass compositions not only dictate the coordination in glass network structures but may also exert a profound influence on the valence states of cations. It is widely acknowledged that the presence of Tb^{4+} ions is detrimental to MO performance. Multiple studies have demonstrated that the valence of Tb can be significantly impacted by optical basicity, network structure, and mixed valence elements. For instance, Al_2O_3 has been identified as a proficient electron donor, capable of reducing Tb^{4+} to Tb^{3+} owing to its high optical basicity [12]. Moreover, modulations in [BO_3] and [BO_4] units can alter the glass network structure and potentially impact the Tb valence state [13, 14]. Given that only Tb^{3+} exhibits MO response, optimizing MO performance through glass composition to increase Tb^{3+} concentration is highly effective.

In this work, borogermanate glass was selected as the matrix, where GeO_2 acts as glass network former that effectively preserves amorphous structure connectivity. B_2O_3 is the most extensively studied glass composition, which not only facilitates the melting process but also confers flexible coordination to maintain network connectivity [15-17]. To elucidate the diverse effects of distinct compositions, Tb-Ge-B-Ga (TGBG) and Tb-Ge-B-La (TGBL) glasses were synthesized and subjected to comparative analysis. It is noteworthy that Ga_2O_3 and La_2O_3 serve as a

network modifier and network intermediate, respectively. Their roles in network structure and regulation of Tb valence are obviously disparate. By increasing the Tb_2O_3 concentration from 20 mol.% to 45 mol.%, MO glass shows an outstanding Verdet constant of 105 rad/(T·m) at 650 nm. This work will serve as an invaluable reference for optimizing the composition of MO glass devices.

2. Experimental

2.1. Magneto-optical glass preparation

The MO glasses investigated were fabricated utilizing the melt-quenching technique. Based on these compositions, the MO glasses were categorized into TGBG and TGBL. All of the raw materials, including Tb_4O_7 (99.999%), GeO_2 (99.999%), H_3BO_3 (99.999%), Ga_2O_3 (99.999%), and La_2O_3 (99.999%), were accurately weighed according to the specified molar ratios outlined in **Table 1**. After grinding and mixing in a mortar for 30 min, the thoroughly mixed raw material powder was carefully transferred to a corundum crucible and then the crucible subjected to a lifting furnace for the melting process, which was meltd at 1450 ^oC for 90 min. To prevent crystallization, the melt was poured over a graphite plate preheated to 300 ^oC and quickly pressed into discs. Subsequently, these glass discs were transferred to an annealing furnace where they were annealed at 550 ^oC for 2 h and then gradually cooled to room temperature. The prepared MO glasses were characterized after polishing, enabling a comprehensive evaluation of their properties and performance.

Table 1 Compositions of MO glasses

Abbreviation	GeO_2 (mol.%)	B_2O_3 (mol.%)	Tb_2O_3 (mol.%)	La_2O_3 (mol.%)	Ga_2O_3 (mol.%)
20T20L	15	45	20	20	
20T25L	15	40	20	25	
20T30L	15	35	20	30	
30T10L	15	45	30	10	
40T5L	15	40	40	5	
45T5L	15	35	45	5	
20T20G	15	45	20		20
20T25G	15	40	20		25
20T30G	15	35	20		30
30T10G	15	45	30		10
40T5G	15	40	40		5
45T5G	15	35	45		5

2.2 Characterization

The glass structure was characterized by Fourier transformed infrared spectrometer (FTIR, INVENIO S) and Raman spectra. For the FTIR, the glass was ground into powder and mixed with ultradry KBr powder at a ratio of 1:100, then pressed into a thin slide for testing. The slide was tested in the range of 400-1600 cm^{-1}. Raman spectra were recorded on Raman spectrometer (LABHRev-UV) in the 20-1500 cm^{-1} range. The excitation laser wavelength is 532 nm. To avoid the glass damage, a 25% neutral density filter was used.

The valence state of Tb ions in the glass was measured by X-ray photoelectron spectroscopy (XPS, JPC-9010MC, JEOL) with Mg-Kα as the X-ray source. The binding energies from the XPS measurements were calibrated with reference to the C 1s.

Based on Archimedes principle, the density (ρ) of Tb-doped glass samples was determined with deionized water and calculated with the following formula,

$$\rho = \frac{m_g \cdot \rho_{water}}{(m_g - m_0)} \quad (1)$$

where m_g and m_0 are the weight of the glass in the air and the water, respectively. ρ_{water} is the density of water.

The optical transmittance of glass was measured by the ultraviolet-visible-near infrared (UV-Vis-NIR) spectrophotometer (UH4150, HITACHI, Japan) in the 200-1650 nm range. The photoluminescence (PL) was measured by an assembled optical system (QuantaMaster/TimeMaster/Near-infrared).

The Faraday rotation angle was measured at room temperature using a commercial measurement setup (FD-FZ-C, Fudan Tianxin, Shanghai). The light source was a 650 nm semiconductor laser. The max external magnetic field was 1.35 T. Besides, the Verdet constant (V) can be calculated with the formula,

$$V = \theta / Bd \quad (2)$$

where θ is the rotation angle, B is the magnetic flux density, and d is the sample thickness.

3. Results and discussion

3.1. Structural analysis

Through the melt-quenching method, two series of Tb-doped borogermanate glasses were prepared. The pictures of these glasses are shown in **Figure S1**. The bonds of B_2O_3 and GeO_2 were disrupted to form the primary network structure. Furthermore, Ga_2O_3 and La_2O_3 served as network modifier and intermediate, respectively with different roles in the structure. In the present glass, the Ga^{3+} and La^{3+} ions were linked to the network through bridge oxygen [18, 19]. Increasing

Ga_2O_3 may interrupt the original network structure, but potentially prevent Tb from aggregating. Conversely, as La has a similar radius to Tb, increasing La_2O_3 may form La-O bonds to construct a new network structure.

To validate our hypothesis, the B_2O_3 were partially substituted with La_2O_3 and Ga_2O_3 in glasses containing 20 mol.% Tb_2O_3. Then the network structure changes were assessed using Fourier-transform infrared spectroscopy (FTIR). The normalized FTIR absorption spectra of the TGBL and TGBG glasses are depicted in **Figures 1a** and **1b**, respectively. Multiple vibration bands are marked and classified into three regions: (i) vibrations of Ge-O-Ge, La-O, and B-O-B between 400 and 800 cm^{-1}, (ii) B-O vibrations of the [BO_4] tetrahedral units between 900 and 1200 cm^{-1}, and (iii) B-O vibrations of the [BO_3] triangular units between 1200-1500 cm^{-1} [20-25]. As shown in **Figure 1a**, the absorption peaks at approximately 1500 cm^{-1} and 900-1200 cm^{-1} decreased with the decrease of B_2O_3 and the increase of La_2O_3, indicating a reduction in pyroborate and [BO_4] units [26, 27]. Conversely, the peaks around 1350 cm^{-1} increase, suggesting an increase in [BO_3] units within boroxol rings, such as meta- and orthoborate groups [26-30]. The peaks related to Ge-O-Ge vibrations between 400-750 cm^{-1} exhibit minimal changes, indicating that adding La_2O_3 has little impact on the Ge-O network [31, 32]. In **Figure 1b**, as B_2O_3 content decreases and Ga_2O_3 content increases, a noticeable decrease in the peaks associated with [BO_4] units (900-1200 cm^{-1}), borate groups (800-900 cm^{-1}), and Ge-O networks (400-750 cm^{-1}) is observed. This indicates the disruption of the original glass network and a decrease in glass network connectivity [26].

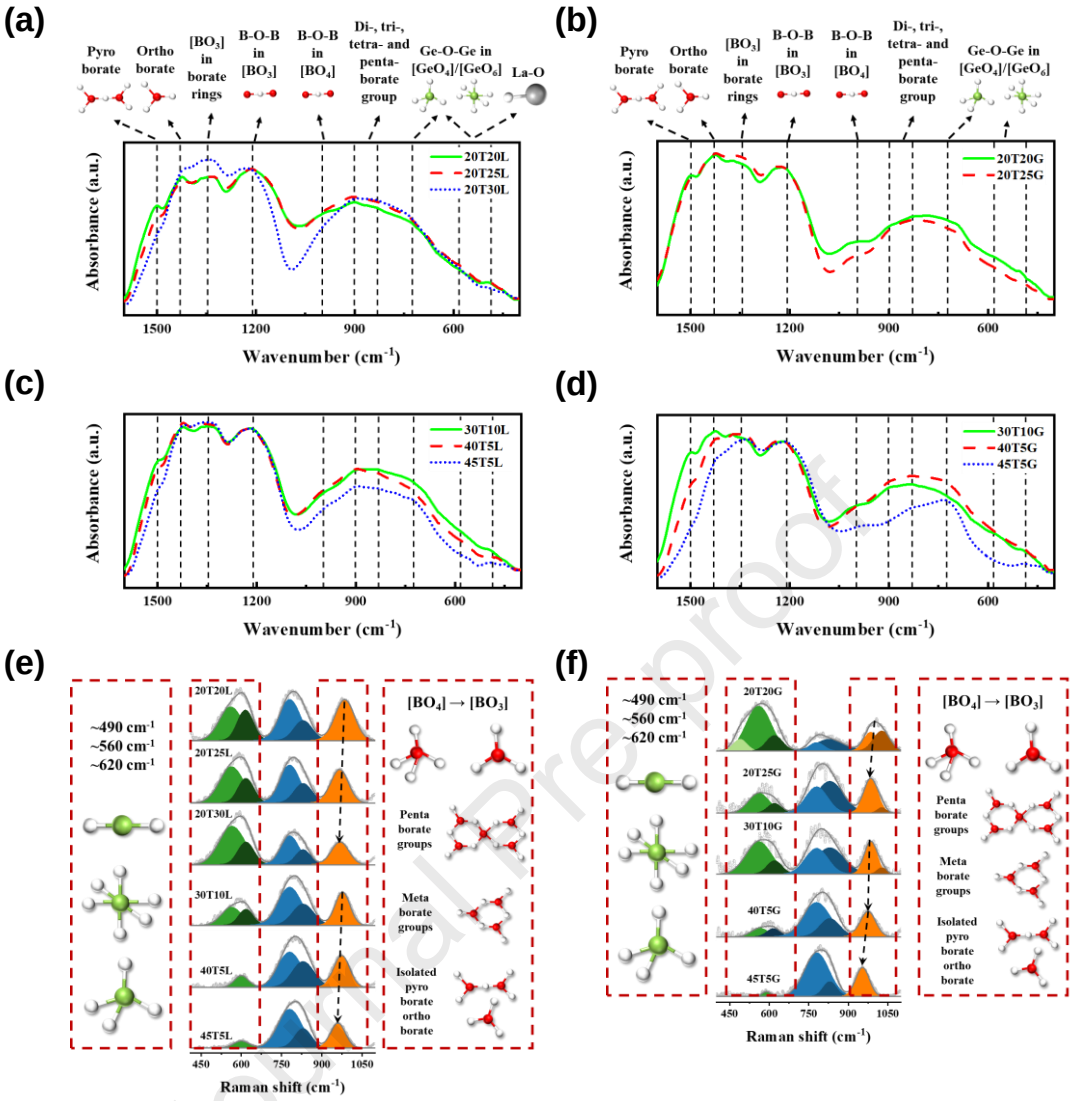

Figure 1. Normalized FTIR spectra of (a) TGBL and (b) TGBG MO glasses with the increase of La_2O_3 and Ga_2O_3 (Normalized at 1215 cm^{-1}). Normalized FTIR spectra of (c) TGBL and (d) TGBG MO glasses with the increase of Tb_2O_3 (Normalized at 1215 cm^{-1}). Deconvolution of Raman spectra of (e) TGBL and (f) TGBG MO glasses, respectively.

In addition, the FTIR spectra of TGBL and TGBG glasses were analyzed with the increase of Tb_2O_3 content as shown in **Figures 1c** and **1d**, respectively. As the Tb_2O_3 increases from 30 mol.% to 45 mol.%, the peaks at 1500 cm^{-1}, 800-1200 cm^{-1}, and 400-750 cm^{-1} decrease, indicating a reduction in the breakage of B-O and Ge-O

bonds within the glass network [26, 28]. Significantly, the peaks in the 1350-1600 cm^{-1} range of TGBG glasses exhibit a more pronounced decrease than that of TGBL glasses. This effect can be attributed to the network modifier nature of Ga_2O_3. As the content of Ga_2O_3 increases, the glass network becomes more prone to breakage, particularly affecting the bonds between boroxol rings. On the other hand, La_2O_3, being a network intermediate, has a minimal impact on the glass network. Similarly, the intensity of peaks in the 800-1200 cm^{-1} and 400-750 cm^{-1} ranges of TGBG glasses shows a more pronounced decrease. This further indicates that Ga_2O_3 has a more significant influence in disrupting the germanium boron oxide glass network.

To further support the findings obtained from FTIR analysis, Raman spectra of MO glasses were conducted. **Figures 1e** and **1f** present the Raman spectra of the glasses after deconvolution for overlap peaks. The peaks observed between 450-670 cm^{-1} originate from the vibration of Ge-O-Ge in [GeO_4] and [GeO_6] units [19, 33]. Consistent with the FTIR results, these peaks show minimal changes with increasing La_2O_3 content. On the other hand, the intensity of the Ge-O peaks decreases with the increase of Ga_2O_3 content, indicating the Ge-O bond is broken. The peaks observed between 670-900 cm^{-1} correspond to the boroxol rings with varying numbers of [BO_4] units, ranging from none to two [24, 34-36]. Another region of Raman peaks between 900-1070 cm^{-1} primarily represents the vibration of B-O bonds in [BO_3] and [BO_4] units [24, 37]. As La_2O_3, Ga_2O_3, and Tb_2O_3 content increases, these peaks exhibit a noticeable shift from the right to the left in the spectrum. According to the references [34, 38-40], this shift indicates the transformation of [BO_4] units to [BO_3] units,

signifying a shift from a more polymerized boroxol ring to a less polymerized boroxol network.

Generally, the addition of La_2O_3 introduces La-O bonds into the network structure. Due to the comparable radius and concentration of Tb (r=0.092 nm) and La (r=0.106 nm) ions, the structure remains relatively stable. However, when the La_2O_3 contents increase, a significant decrease in [BO_4] units can be observed in the 20T30L glass. Excessive La incorporation weakens the network structure excessively, leading to the breakage of B-O bonds. On the other hand, Ga_2O_3 has a disruptive effect on the original glass network. This is evident from the decrease in peaks associated with B-O and Ge-O networks, indicating a disruption in network connectivity [41]. This reflects that TGBL glass has a stronger network connectivity than TGBG. Furthermore, an increase in Tb_2O_3 content results in substantial disruption of the original glass network. The Ge-O-Ge peaks decrease significantly, and pentaborate species undergo depolymerization, transitioning into isolated pyro- and orthoborates.

3.2. Mechanism of valance change in MO glasses

The MO property of glass predominantly stems from the presence of Tb^{3+} ions. However, Tb^{3+} and Tb^{4+} ions coexist in the glass during high-temperature melting process. Given the potential influence of varying compositions on the distribution of valence states, quantitative analysis becomes imperative. Accordingly, this discussion focuses primarily on the valence state within the MO glass, aiming to elucidate the implications of such variability.

3.2.1. Valence state of Tb and Ge

The assessment of Tb ion states can be quantitatively determined through the excitation of the 3d orbitals using a focused X-ray beam. It is noteworthy that GeO_2 serves as a crucial network former within the glass, and the presence of Ge ions in a mixed valence state can significantly impact both the network structure and the state of Tb ions. Consequently, the evaluation of the valence state of Ge ions is also conducted to elucidate the intricate relationship between the network structure and the state of Tb ions.

The X-ray photoelectron spectroscopy (XPS) spectra of Ge 3d and Tb 3d are presented in **Figures 2a** and **2c**, respectively. Based on established literatures [?], the deconcolution of these peaks were conducted. In the Ge 3d spectra, the observed binding energies at approximately 29, 31.6, and 32.5 eV correspond to Ge^0, Ge^{2+}, and Ge^{4+} states, respectively [42, 43]. Similarly, in the Tb 3d spectra, the fitting peaks can be divided into two categories: Tb^{3+} (~1239, ~1263, and ~1274 eV) and Tb^{4+} (~1241, ~1243, ~1251, ~1276, and ~1278 eV) [44, 45]. The quantitative distributions of Ge and Tb ion valences are summarized in **Figures 2b** and **2d**, respectively. Based on the observations in **Figure S2**, it is evident that the calculated valence of Ge decreases with the increase of Ga_2O_3 and La_2O_3. Similarly, with the increase of Tb_2O_3, the calculated valence of Ge also decreases. These findings indicate that when La_2O_3 and Ga_2O_3 replace B_2O_3, electrons tend to enter the Ge ions, resulting in a decrease in the calculated valence of Ge. Furthermore, the calculated valence of Tb also changes with the increase of Ga_2O_3, La_2O_3, and Tb_2O_3. This variation signifies the transformation from Tb^{4+} to Tb^{3+} ions in the glass. Notably, the proportion of Tb^{3+} among the Tb ions

is higher in TGBL glasses than that in other glass matrices.

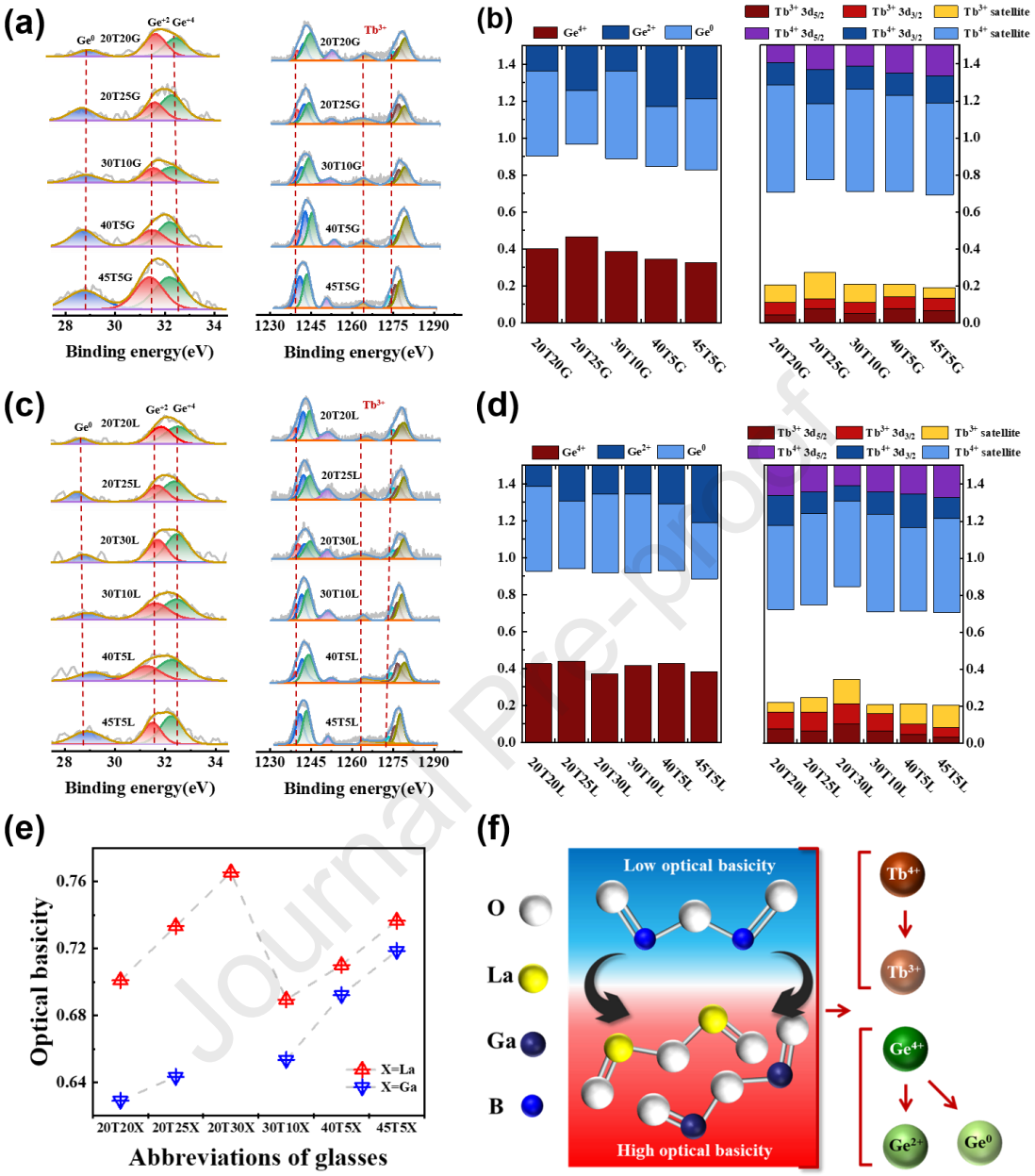

Figure 2. Ge 3d and Tb 3d XPS spectra of (a) TGBG and (c) TGBL glasses, quantitative analysis of Ge and Tb ions with different valence states in (b) TGBG and (d) TGBL glasses, (e) optical basicity of TGBG and TGBL MO glasses, (f) mechanism of ion exchange between Tb and Ge ions

3.2.2. Electron transfer mechanism in MO glasses

To understand the electron transfer mechanism occurring in MO glass, the

optical basicity (Λ_{th}) was calculated using the **Formula S6**. **Figure 2e** visually presents the optical basicity values for TGBG and TGBL glasses. As elucidated by Duffy, Λ_{th} serves as an indicator of the electron transfer capacity across various oxides. Notably, **Figure 2e** reveals that the Λ_{th} value of TGBL exceeds that of TGBG, implying a higher electron-donor ability within TGBL. Consequently, the reduction of Tb^{4+} to Tb^{3+} is facilitated to a greater extent in TGBL, which aligns consistently with the XPS results.

Due to the higher Λ_{th} of Ga_2O_3 and La_2O_3 compared to B_2O_3, an increased substitution of Ga_2O_3 and La_2O_3 in place of B_2O_3 results in a greater influx of electrons into the glass network. The replacement path is illustrated in **Figure 2f**. Based on the calculated valence states of Ge and Tb ions, the processes of "Ge^{4+}→low valence Ge" and "Tb^{4+}→Tb^{3+}" occur simultaneously. Due to the lower ionization energies of Tb (1st/2nd/3rd/4th: 565.77/1110.8/2110/3790 kJ/mol) compared to that of Ge (1st/2nd/3rd/4th: 762.18/1537.46/3286.1/4410.9 kJ/mol), the dominant process is the reduction of Ge^{4+} to low valence Ge. Additionally, the lower valence Ge ions exist in the amorphous state within the glass network [46, 47]. The Λ_{th} value exhibits a proportional increase with the increase of Tb_2O_3 content. However, the high optical basicity of Tb_2O_3 renders Tb^{3+} ions susceptible to electron loss and oxidation to Tb^{4+} ions. Consequently, the proportion of Tb^{3+} ions decreases with the increase of Tb content.

3.3. Optical properties

3.3.1. Transmission and absorption spectra of MO glasses

Given its transparent nature, the optical transmittance of a glass material plays a crucial role in minimizing optical signal loss, thereby enhancing its suitability for various optical applications. **Figures 3a** and **3b** provide a comprehensive depiction of the transmission and absorption spectra for TGBL glasses (the spectra of TGBG glasses are shown in **Figures S3a and S3b** for comparison). The distinctive absorption peak observed at 483 nm can be attributed to the $^7F_6 \rightarrow {}^5D_4$ electron transition of Tb^{3+} ions. As the concentrations of Ga_2O_3 and La_2O_3 increase, the average transmittance of TGBG and TGBL glasses, both containing 20 mol.% Tb_2O_3, reaches 82.44% and 85.07%, respectively, within the wavelength range of 500 to 1600 nm. While TGBL glass exhibits higher overall transmittance, its transmittance within the 400 to 500 nm range falls below that of TGBG glass. Moreover, increasing amounts of La_2O_3 lead to a red shift of the absorption edge within the ultraviolet (UV) region.

To elucidate the underlying mechanism behind the shift in the absorption edge, the band gap (E_g) was calculated, as depicted in **Figure 3c** and **Figure S4**. It is evident from the results that E_g exhibits a decreasing trend with the increasing concentrations of Ga_2O_3 and La_2O_3. This phenomenon can be attributed to the linear relationship between the upper edge of the valence band and the absence of p-electron pairs on the oxygen-bridging atoms. As the bonding energy increases, the E_g enlarges. Considering that both Ga_2O_3 and La_2O_3 disrupt the glass network, the oxygen atoms bonded to La and Ga can be regarded as non-bridging oxygen. Consequently, with the increasing amounts of Ga_2O_3 and La_2O_3, the bond strength between Ga/La and

oxygen ions intensifies, resulting in a weakened bond between the network formers and oxygen-bridging atoms. This, in turn, leads to a gradual blue shift of the absorption edge in the UV region, corresponding to lower wavelengths. Notably, given that the bond energy of La-O (~799 kJ/mol) surpasses that of Ga-O (~353 kJ/mol), the E_g of TGBL glasses is comparatively lower.

Observing **Figure 3d**, it becomes evident that MO glasses exhibit a gradual browning effect, with the color darkening further as the Tb_2O_3 content increases. Specifically, when the Tb_2O_3 concentration is raised from 30 mol.% to 45 mol.%, the average transmittance of TGBG and TGBL glasses within the wavelength range of 500 to 1600 nm reaches 78.87% and 80.12%, respectively. This phenomenon can be attributed to the weaker bonding between rare earth ions and oxygen ions compared to that between the network-forming ions (Ge and B) and oxygen ions. Consequently, the connectivity of the glass network and the E_g decrease, ultimately resulting in a red shift of the absorption edge within the UV region.

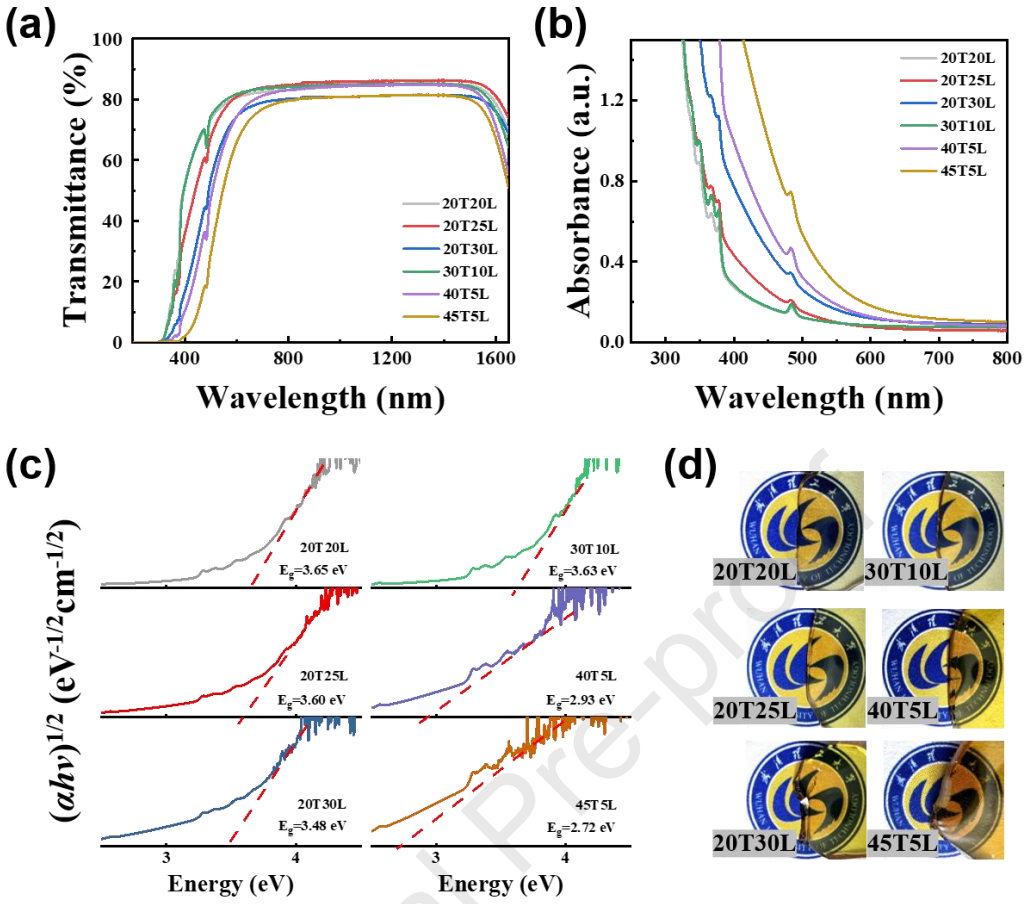

Figure 3. (a) Transmittance and (b) absroption spectra of TGBL glasses, (c) band gap of TGBL glasses, (d) pictures of polished TGBL glasses

3.3.2. Luminescent property of MO glasses

Figures 4a and **4b** show the excitation and emission spectra of TGBL glasses, while corresponding spectra of TGBG glasses can be found in **Figures S3c** and **S3d**. When the monitoring emission wavelength at the 542 nm, the dominant excitation bands for both TGBL and TGBG glasses are observed at specific wavelengths, namely 284, 301, 316, 339, 350, 369, and 375 nm, corresponding to the transitions from ground state $^7F_6$ to excited states $^5H_4$, $^5H_6$, $^5H_7$, $^5L_8$, $^5L_9$, $^5L_{10}$, and $^5D_3$ of Tb^{3+} ions, respectively. Notably, due to the shielding effect of $5s^25p^6$ on the 4f electrons of Tb^{3+} ions, the positions of the excitation bands remain relatively unchanged.

Besides, the luminescence exhibited by MO glasses primarily originates from the energy transition of Tb^{3+} ions, specifically from the $^5D_4$ to ^7F_J states: $^5D_4 \rightarrow {}^7F_6$ (489 nm), $^5D_4 \rightarrow {}^7F_5$ (544 nm), $^5D_4 \rightarrow {}^7F_4$ (585 nm) and $^5D_4 \rightarrow {}^7F_3$ (621 nm) [48]. Notably, under the excitation wavelength of 377 nm, the $^5D_4 \rightarrow {}^7F_5$ transition of Tb^{3+} ions exhibits the highest probability, resulting in the strongest yellow-green fluorescence emission at 544 nm [49-52]. To provide a more comprehensive understanding of the energy transfer process involving Tb^{3+} ions, the energy level transitions of Tb^{3+} ions have been illustrated in **Figure 4e**.

With the increase of Tb_2O_3, the intensity of the excitation band exhibits a gradual decrease. To shed light on this phenomenon, we conducted calculations to determine the critical distance (R_c) between Tb^{3+} ions, as depicted in **Figure S5**. Remarkably, with an increase in Tb^{3+} ion doping concentration, R_c experiences a decrease. Once the concentration of Tb ions surpasses the threshold for luminescence quenching, the probability of energy transfer increases, leading to a cross-relaxation effect known as $^5D_3 + {}^7F_6 \rightarrow {}^5D_4 + {}^7F_0$. This process significantly weakens the luminescence intensity observed. Notably, 20T30L exhibits a notably high luminous intensity, primarily attributed to the conversion of a substantial amount of [BO_4] units to [BO_3], which enhances the dispersion of Tb^{3+} ions within the glass matrix.

Figures 4c and **4d** depict the photoluminescence intensity of glasses doped with equal concentrations of Tb ions, showing the distinct luminescent properties of TGBL and TGBG glasses. Notably, TGBL glass demonstrates a superior luminescence performance compared to TGBG glass. However, as the Tb content increases, TGBG

glasses exhibit higher luminescence intensity in comparison to TGBL glass.

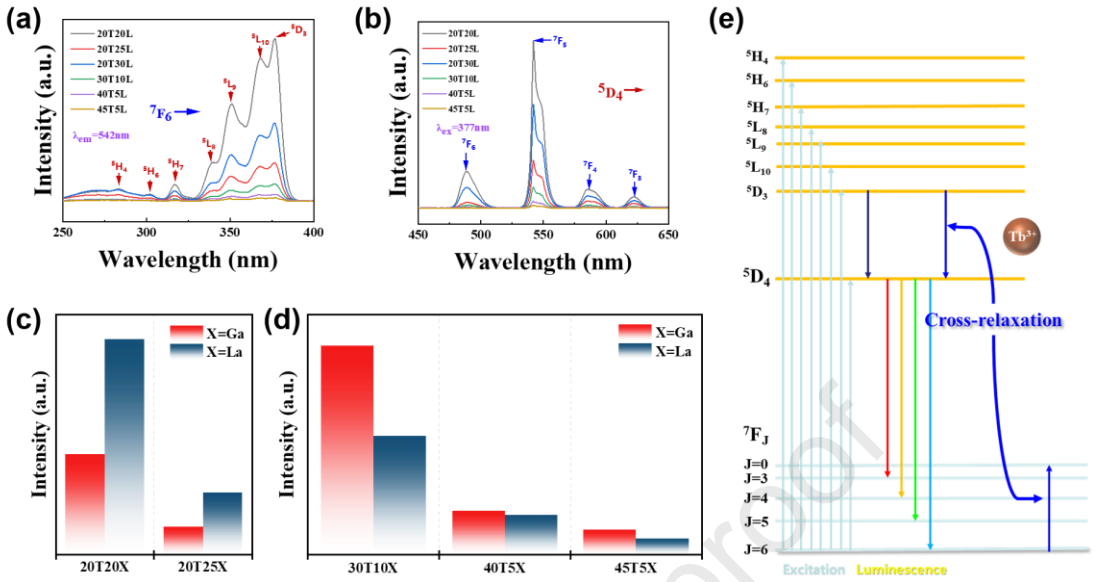

Figure 4. (a) Excitation and (b) emission spectra of TGBL glasses. Comparison of the emission intensity of Tb: $^5D_4 \rightarrow {}^7F_5$ transition between TGBG and TGBL glasses containing (c) 20 mol.% Tb_2O_3 and (d) higher content of Tb_2O_3. (e) Energy transfer process of Tb^{3+}

3.4. Magneto-optical property

The phenomenon where incident light passing through a glass undergoes rotation of the polarization plane in the presence of a magnetic field is known as the Faraday effect. The angle of rotation, denoted as θ, can be determined using the equation $\theta=VBd$, where V represents the Verdet constant, B denotes the magnetic flux density, and d is the thickness of the MO glass. Here, we delve deeper into the relationship between the glass matrix, concentration of Tb^{3+} ions, and the Verdet constant.

3.4.1. Tb^{3+} concentration in MO glasses

The effective concentration of Tb ions (N_{Tb}) signifies the fraction of Tb ions that are successfully incorporated into the glass network [53]. **Figure 5a** illustrates the N_{Tb}

values of MO glasses, calculated using **Formula S7**. The density of MO glasses is essential to calculate N_{Tb}, as shown in **Figure S6**. With the increase in Ga_2O_3 and La_2O_3 content in the MO glasses, there is a corresponding rise in the density of the glasses. However, simultaneously, the mass percentage of the Tb compound (W_c) decreases. Although the density of the glasses increases, the reduction in W_c has a more significant impact, resulting in a decreasing trend observed in N_{Tb}. Generally, N_{Tb} in TGBG is higher than that in TGBL, primarily attributed to the larger atomic mass of La_2O_3. As the Tb_2O_3 content increases, N_{Tb} and the Verdet constant exhibit an upward trend. However, N_{Tb} decreases with the increase of Ga_2O_3 or La_2O_3 content, which is contrary to the trend of the Verdet constant. **Figure 5b** shows the concentration of Tb^{3+} ions (C_{Tb}^{3+}, calculated using **Formula S8**) in the MO glasses. Upon comparing **Formula S7** with **Formula S8**, it becomes evident that N_{Tb} alone cannot accurately reflect the valence distribution among Tb ions. N_{Tb} refers the total concentration of Tb ions that enter the glass network. On the other hand, C_{Tb}^{3+}, as shown in **Formula S8**, incorporates the proportion of Tb^{3+} among Tb ions (P_{Tb}^{3+}) into the calculation, enabling the determination of the amount of Tb^{3+} ions that have entered the glass network. Thus, C_{Tb}^{3+} represents the total concentration of Tb^{3+} ions present in the glass network. Considering the presence of multiple valence states, it is obvious that P_{Tb}^{3+} increases significantly with the rise in Ga_2O_3 and La_2O_3 content in the MO glasses. Consequently, C_{Tb}^{3+} also increases, which is in contrast to the trend observed in N_{Tb}. Notably, C_{Tb}^{3+} aligns with the trend observed for the Verdet constant.

3.4.2. Verdet constant of MO glasses

The Verdet constant serves as the criterion for assessing the MO property of glasses. In **Figure 5c**, the Verdet constant of MO glasses was experimentally measured at a wavelength of 650 nm. Overall, V_{TGBG} surpasses V_{TGBL}, aligning consistently with the N_{Tb} and C_{Tb}^{3+} results. Notably, the composition 45T5G exhibits the highest Verdet constant, reaching 105 rad/(T·m) at 650 nm. The observed increase in Verdet constant with the inclusion of Ga_2O_3 and La_2O_3 can be attributed to the greater incorporation of electrons into the glass network, subsequently leading to higher Tb^{3+} content. Since C_{Tb}^{3+} represents the quantity of Tb^{3+} ions within the MO glass, its correlation with the Verdet constant is notably strong.

Figure 5d presents a comparative analysis of different glass matrices with Tb_2O_3 concentrations of 20 mol.% and 45 mol.%, respectively. When the Tb_2O_3 content is 20 mol.%, TGBG glass exhibits a higher Verdet constant. However, it demonstrates relatively lower Tb^{3+} concentration among Tb ions, and its luminescence intensity is lower as well. Conversely, when the Tb_2O_3 content reaches 45 mol.%, TGBG glass shows a higher luminescence intensity compared to TGBL glass. This investigation reveals that distinct glass matrices possess varying dominant areas in terms of their properties. To achieve optimal performance, compositional adjustments prove to be a viable option.

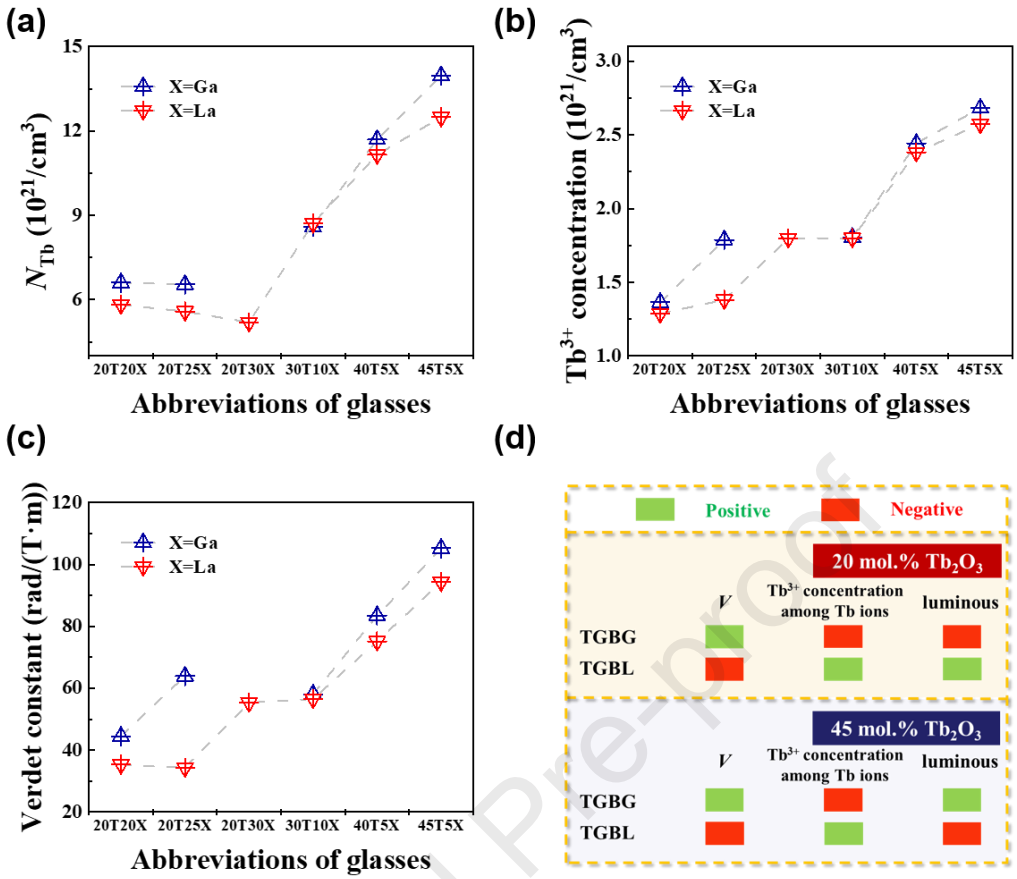

Figure 5. (a) Effective concentration of Tb ions, (b) concentration of Tb^{3+} ions in MO glasses, (c) Verdet constant of MO glasses at 650 nm, (d) properties comparison of MO glasses with the same Tb content

4. Conclusion

In summary, TGBG and TGBL MO glasses were successfully prepared. Combining the optical and MO properties, the glass network structure and valence change mechanism are discussed in detail to clear the effects of Ga_2O_3 and La_2O_3 in glass. In TGBG MO glasses, an increase in Ga_2O_3 content leads to a significant reduction in network connectivity. Higher Ga_2O_3 content can cause glass crystallization, resulting in a loss of permeability. On the other hand, an increase in Tb_2O_3 content in TGBG glasses leads to the highest Verdet constant observed at 650

nm, reaching an impressive value of 105 rad/(T·m). In TGBL MO glasses, the addition of La_2O_3 maintains the glass network connectivity. As the La_2O_3 content increases, the concentration of Tb^{3+} ions among Tb ions also increases. TGBL glasses exhibit a higher Tb^{3+} concentration than TGBG glasses. Furthermore, when the Tb_2O_3 content is around 20-25 mol.%, TGBL glasses exhibit higher luminescence intensity. However, as the Tb_2O_3 content increases, the luminescence intensity of TGBG glasses becomes better. Overall, to obtain better performance, further regulation of Ga_2O_3 and La_2O_3 is a good choice. Glass containing Ga_2O_3 has better MO performance. Adding La_2O_3 into glass could improve optical properties and increase the concentration of Tb^{3+} among Tb ions.

Declaration of competing interest

The authors declare that they have no known competing financial interests or personal relationships that could have appeared to influence the work reported in this paper.

Acknowledgment

Xudong Zhao and Jiadong Li contributed equally to this work. This work is financially supported by the National Natural Science Foundation of China (U2241236, 62275206, 61975156, 52372014).

Supplementary material

The Supplementary material is available at

Figure S1 Pictures of MO glasses; Figure S2 Calculated valence state of Ge and Tb in

(a)TGBG and (b)TGBL glasses; Figure S3 (a) Transmittance and (b) absorption spectra of TGBG MO glasses, (c)excitation and (d)emission spectra of TGBG MO glasses; Figure S4 Band gap of TGBG MO glasses; Figure S5 Critical distance R_c between Tb ions; Figure S6 Density of the MO glasses; Optical basicity; Calculation of the effective concentration of Tb ions; Calculation of Tb^{3+} ions concentration.

References

[1] T. Hayakawa; M. Nogami; N. Nishi and N. Sawanobori, Faraday rotation effect of highly Tb_2O_3/Dy_2O_3-concentrated B_2O_3-Ga_2O_3-SiO_2-P_2O_5 glasses, Chem. Mater. 14 (2002) 3223-3225.

[2] K. J. Carothers; R. A. Norwood and J. Pyun, High Verdet constant materials for magneto-optical faraday rotation: A review, Chem. Mater. 34 (2022) 2531-2544.

[3] H. Yin; Y. Gao; Y. Gong; R. Buchanan; J. Song and M. Li, Wavelength dependence of Tb^{3+} doped magneto-optical glass Verdet constant, Ceram. Int. 44 (2018) 10929-10933.

[4] Q. Wang; S. Song; N. Nie; J. Tan and W. Wang, Luminescent $NaTb(SO_4)_2$ nanoprobe for hydrogen peroxide based on switchable fluorescence of Tb(IV)/Tb(III) redox couple, Ceram. Int. 47 (2021) 18942-18947.

[5] H. Cheng; B. Lu; Y. Liu; Y. Zhao; Y. Sakka and J.-G. Li, Transparent magneto-optical Ho_2O_3 ceramics: Role of self-reactive resultant oxyfluoride additive and investigation of vacuum sintering kinetics, Ceram. Int. 45 (2019) 14761-14767.

[6] J. F. Barry; D. J. McCarron; E. B. Norrgard; M. H. Steinecker and D. DeMille, Magneto-optical trapping of a diatomic molecule, Nature 512 (2014) 286-289.

[7] T. Higo; H. Y. Man; D. B. Gopman; L. Wu; T. Koretsune; O. M. J. van't Erve; Y. P. Kabanov; D. Rees; Y. F. Li; M. T. Suzuki; S. Patankar; M. Ikhlas; C. L. Chien; R. Arita; R. D. Shull; J. Orenstein and S. Nakatsuji, Large magneto-optical Kerr effect and imaging of magnetic octupole domains in an antiferromagnetic metal, Nat. Photonics 12 (2018) 73-78.

[8] M. A. Schmidt; L. Wondraczek; H. W. Lee; N. Granzow; N. Da and P. S. J. Russell, Complex Faraday rotation in microstructured magneto-optical fiber waveguides, Adv. Mater. 23 (2011) 2681-2688.

[9] H. Lin; B. Liu; L. Zhou; H. Yang; J. He; T. Zhang; H. Liu; X. Jiang; C. Li; S. Li; L. Liu; F. Zeng and Z. Su, Enhancements of magneto-optical properties of GeO_2-PbO-B_2O_3-SiO_2-P_2O_5 glass doped Tb^{3+} ion, Mater. Chem. Phys. 282 (2022) 125963.

[10] H. Yang and Z. Zhu, Magneto-optical glass mixed with Tb^{3+} ions: high Verdet constant and luminescence properties, J. Lumin. 231 (2021) 117804.

[11] H. Jia and Z. Zhu, Concentration-wavelength dependence of magneto-optical properties in Tb^{3+}-doped BGAP glass, J. Non-Cryst. Solids 552 (2021) 120456.

[12] X. Zhao; W. Li; Q. Xia; P. Lu; H. Tao; M. Xia; X. Zhang; X. Zhao and Y. Xu, High Verdet constant glass for magnetic field sensors, ACS Appl. Mater. Interfaces 14 (2022) 57028-57036.

[13] Y. Zhang; S. Murai; A. Maeno; H. Kaji; M. Shimizu; Y. Shimotsuma; Z. Ma; J. Qiu and K. Tanaka, Microstructure and Faraday effect of Tb_2O_3-Al_2O_3-SiO_2-B_2O_3 glasses for fiber-based magneto-optical applications, J. Am. Ceram. Soc. 105 (2021) 1198-1209.

[14] H. Yin; Y. Gao; H. Guo; C. Wang and C. Yang, Effect of B_2O_3 content and microstructure on Verdet constant of Tb_2O_3-doped GBSG magneto-optical Glass, J. Phys. Chem. C 122 (2018) 16894-16900.

[15] J. Zeng; H. Zhu; Y. Ding; D. Zhang; Y. Dai; Y. Wang; J. Chen; F. Wang and Q. Liao, Effects of Al_2O_3 and B_2O_3 on the structural features of iron phosphate glasses, J. Mol. Struct. 1261 (2022) 132928.

[16] D. F. Franco; Y. Ledemi; W. Correr; S. Morency; C. R. M. Afonso; S. H. Messaddeq; Y. Messaddeq and M. Nalin, Magneto-optical borogermanate glasses and fibers containing Tb^{3+}, Sci. Rep. 11 (2021) 9906.

[17] M. C. Dinca; B. A. Sava; A. C. Galca; V. Kuncser; N. Iacob; G. E. Stan; L. Boroica; A. V. Filip and M. Elisa, Magneto-optical properties of borophosphate glasses co-doped with Tb^{3+} and Dy^{3+} ions, J. Non-Cryst. Solids 2021 568 (2021) 120967.

[18] D. F. Franco; R. G. Fernandes; S. H. Santagneli; M. de Oliveira; H. Eckert and M. Nalin, Structural study of the germanium-aluminum-borate glasses by solid state NMR and raman spectroscopies, J. Phys. Chem. C 124 (2020) 24460-24469.

[19] O. N. Koroleva; M. V. Shtenberg; R. T. Zainullina; S. M. Lebedeva and L. A. Nevolina, Vibrational spectroscopy and density of K_2O-B_2O_3-GeO_2 glasses with variable B/Ge ratio, Phys. Chem. Chem. Phys. 21 (2019) 12676-12684.

[20] K. S. Shaaban; B. M. Alotaibi and E. S. Yousef, Effect of La_2O_3 Concentration on the Structural, Optical and radiation-shielding behaviors of titanate borosilicate glasses, J. Electron. Mater. 52 (2023) 3591-3603.

[21] T. Lan; T. Han; D. Jiang; Y. Wen; X.-Y. Sun; Z. Hua; S. Qian; H. Ban; H. Cai; J. Han; H. Liu; S. Liu; L. Ma; L. Qin; J. Ren; G. Tang; Z. Wang; Z. Wang and Y. Zhu, Study on the luminescent properties of Eu^{3+}-doped TeO_2-GeO_2-BaO scintillation glasses, Opt. Mater. 133 (2022) 113000.

[22] P. M. Vinaya Teja; C. Rajyasree; S. B. Murali Krishna; C. Tirupataiah and D. Krishna Rao, Effect of Some VA Group Modifiers on R_2O_3 (R=Sb, Bi)-ZnF_2-GeO_2 Glasses doped with CuO by means of spectroscopic and dielectric investigations, Mater. Chem. Phys. 133 (2012) 239-248.

[23] H. A. El Batal; F. H. El Batal; M. A. Azooz; M. A. Marzouk; A. A. El Kheshen; N. A. Ghoneim; F. M. Ezz El Din and A. M. Abdelghany, Comparative shielding behavior of binary PbO-B_2O_3 and Bi_2O_3-B_2O_3 glasses with high heavy metal oxide contents towards gamma irradiation revealed by collective optical, FTIR and ESR measurements, J. Non-Cryst. Solids 572 (2021) 121090.

[24] P. Kaur; K. J. Singh; S. Thakur; P. Singh and B. S. Bajwa, Investigation of bismuth borate glass system modified with barium for structural and gamma-ray

shielding properties, spectrochim. Acta A Mol. Biomol. Spectrosc. 206 (2019) 367-377.

[25] I. Ardelean; S. Cora and D. Rusu, EPR and FT-IR spectroscopic studies of Bi_2O_3-B_2O_3-CuO Glasses, Physica B Condens. Matter 403 (2008) 3682-3685.

[26] L. Bolundut; L. Pop; M. Bosca; G. Borodi; L. Olar; R.-C. Suciu; P. Pascuta; E. Culea and R. Stefan, Structural and spectroscopic properties of some neodymium-boro-germanate glasses and glass ceramics embedded with silver nanoparticles, Ceram. Int. 43 (2017) 12232-12238.

[27] K. A. Naseer; K. Marimuthu; K. A. Mahmoud and M. I. Sayyed, Impact of Bi_2O_3 modifier concentration on barium-zincborate glasses: physical, structural, elastic, and radiation-shielding properties, Eur. Phys. J. Plus 136 (2021) 116.

[28] K. A. Naseer; K. Marimuthu; M. S. Al-Buriahi; A. Alalawi and H. O. Tekin, Influence of Bi_2O_3 concentration on barium-telluro-borate glasses: physical, structural and radiation-shielding properties, Ceram. Int. 47 (2021) 329-340.

[29] H. M. H. Zakaly; H. A. Saudi; S. A. M. Issa; M. Rashad; A. I. Elazaka; H. O. Tekin and Y. B. Saddeek, Alteration of optical, structural, mechanical durability and nuclear radiation attenuation properties of barium borosilicate glasses through BaO reinforcement: experimental and numerical analyses, Ceram. Int. 47 (2021) 5587-5596.

[30] G. Lakshminarayana; K. M. Kaky; S. O. Baki; A. Lira; P. Nayar; I. V. Kityk and M. A. Mahdi, Physical, structural, thermal, and optical spectroscopy studies of

TeO_2-B_2O_3-MoO_3-ZnO-R_2O (R=Li, Na, and K)/MO (M=Mg, Ca, and Pb) glasses, J. Alloys Compd. 690 (2017) 799-816.

[31] B. Kukliński; D. Wileńska; S. Mahlik; K. Szczodrowski; M. Grinberg and A. M. Kłonkowski, Luminescent GeO_2-Pb-Bi_2O_3 glasses co-doped with Tb^{3+1} and Eu^{3+}: excitation energy transfer and color chromaticity, Opt. Mater. 36 (2014) 633-638.

[32] P. Pascuta and E. Culea, FTIR spectroscopic study of some bismuth germanate glasses containing gadolinium ions, Mater. Lett. 62 (2008) 4127-4129.

[33] C. Liu; Y. Zhuang; J. Han; J. Ruan; C. Liu and X. Zhao, Multi-band near-infrared emission in low concentration bismuth doped alkaline earth alumino-boro-germanate glass, Ceram. Int. 46 (2020) 15544-15553.

[34] T. To; A. A. K. R. K. Olsen; B. A. Hansen; K. M. Enevoldsen; V. Lütken; L. R. Jensen; R. E. Youngman and M. M. Smedskjaer, Comparing the effects of Ga_2O_3 and Al_2O_3 on the structure and mechanical properties of sodium borate glasses, J. Non-Cryst. Solids 618 (2023) 122506.

[35] G. Padmaja and P. Kistaiah, Infrared and Raman spectroscopic studies on alkali borate glasses: evidence of mixed alkali effect, J. Phys. Chem. A 113 (2009) 2397-2404.

[36] S. Arunkumar and K. Marimuthu, Concentration effect of Sm^{3+} ions in B_2O_3-PbO-PbF_2-Bi_2O_3-ZnO glasses - structural and luminescence investigations, J. Alloys Compd. 565 (2013) 104-114.

[37] E. Buixaderas; E. M. Anghel; I. Atkinson; P. Simon; V. Bratan and S. Petrescu, Combustion synthesis and structural characterization of the TiB_2-($Na_2O{\cdot}2B_2O_3$-Al_2O_3) composites, Ceram. Int. 41 (2015) 2680-2689.

[38] H. Fan; G. Wang and L. Hu, Infrared, Raman and XPS spectroscopic studies of Bi_2O_3-B_2O_3-Ga_2O_3 glasses, Solid State Sci. 11 (2009) 2065-2070.

[39] B. N. Meera and J. Ramakrishna, Raman spectral studies of borate glasses, J. Non-Cryst. Solids 159 (1993) 1-21.

[40] I. N. Chakraborty and R. A. Condrate, The Vibrational spectra of B_2O_3-GeO_2 glasses, J. Non-Cryst. Solids 81 (1986) 271-284.

[41] Y. Zhang; S. Murai; A. Maeno; H. Kaji; M. Shimizu; Y. Shimotsuma; Z. Ma; J. Qiu and K. Tanaka, Microstructure and Faraday effect of Tb_2O_3-Al_2O_3-SiO_2-B_2O_3 glasses for fiber-based magneto-optical applications, J. Am. Ceram. Soc. 105 (2021) 1198-1209.

[42] A. F. Zatsepin; D. A. Zatsepin; I. S. Zhidkov; E. Z. Kurmaev; H. J. Fitting; B. Schmidt; A. P. Mikhailovich and K. Lawniczak-Jablonska, Formation of Ge^0 and GeO_x nanoclusters in Ge^+-implanted SiO_2/Si thin-film heterostructures under rapid thermal annealing, Appl. Surf. Sci. 349 (2015) 780-784.

[43] H. Takebe; H. Maeda and K. Morinaga, Compositional variation in the structure of Ge-S glasses, J. Non-Cryst. Solids 291 (2001) 14-24.

[44] G. Blanco; J. M. Pintado; S. Bernal; M. A. Cauqui; M. P. Corchado; A. Galtayries; J. Ghijsen; R. Sporken; T. Eickhoff and W. Drube, Influence of the nature of the noble

metal (Rh,Pt) on the low-temperature reducibility of A Ce/Tb mixed oxide with application as TWC component, Surf. Interface Anal. 34 (2002) 120-124.

[45] I. M. Nagpure; S. S. Pitale; E. Coetsee; O. M. Ntwaeaborwa; J. J. Terblans and H. C. Swart, Low voltage electron induced cathodoluminescence degradation and surface characterization of $Sr_3(PO_4)_2$:Tb phosphor, Appl. Surf. Sci. 257 (2011) 10147-10155.

[46] M. Anisuzzaman; N. Ab Manaf; S. Saharudin; K. Yasui and A. Manaf Hashim, A study of stoichiometric composition of Ge thermal oxide by X-ray photoelectron spectroscopic depth profiling, Mater. Today: Proceedings 7 (2019) 619-624.

[47] Y. Negishi; S. Nagao; Y. Nakamura; A. Nakajima; S. Kamei and K. Kaya, Visible photoluminescence of the deposited germanium–oxide prepared from clusters in the gas phase, J. Appl. Phys. 88 (2000) 6037-6043.

[48] G. Gao; A. Winterstein-Beckmann; O. Surzhenko; C. Dubs; J. Dellith; M. A. Schmidt and L. Wondraczek, Faraday rotation and photoluminescence in heavily Tb^{3+}-Doped GeO_2-B_2O_3-Al_2O_3-Ga_2O_3 glasses for fiber-integrated magneto-optics, Sci. Rep. 5 (2015) 8942.

[49] C. Zuo; J. Huang; S. Liu; A. Xiao; Y. Shen; X. Zhang; Z. Zhou and L. Zhu, Luminescence and energy transfer of Tb^{3+}-doped BaO-Gd_2O_3-Al_2O_3-B_2O_3-SiO_2 glasses, Spectrochim. Acta A Mol. Biomol. Spectrosc. 187 (2017) 181-185.

[50] K. Linganna; V. B. Sreedhar and C. K. Jayasankar, Luminescence properties of Tb^{3+} ions in zinc fluorophosphate glasses for green laser applications, Mater. Res. Bull. 67 (2015) 196-200.

[51]P. Dharmaiah; C. S. D. Viswanath; C. Basavapoornima; K. V. Krishnaiah; C. K. Jayasankar and S.-J. Hong, Luminescence and energy transfer in Dy^{3+}/Tb^{3+} co-doped transparent oxyfluorosilicate glass-ceramics for green emitting applications, Mater. Res. Bull. 83 (2016) 507-514.

[52]W. Luo; S. Yan and J. Zhou, Ceramic-based dielectric metamaterials, Interdiscip. Mater. 1 (2022) 11-27.

[53]J. Ding; P. Man; Q. Chen; L. Guo; X. Hu; Y. Xiao; L. Su; A. Wu; Y. Zhou and F. Zeng, Influence of Tb^{3+} concentration on the optical properties and Verdet constant of magneto-optic ABS-PZZ glass, Opt. Mater. 69 (2017) 202-206.

Declaration of interests

☒ The authors declare that they have no known competing financial interests or personal relationships that could have appeared to influence the work reported in this paper.

☐ The authors declare the following financial interests/personal relationships which may be considered as potential competing interests: